All-polyamide nanofibrillar composites by in situ fibrillation of aramid fibers

Nicolas Candau, Sylvain Galland, Oguzhan Oguz, Pascal Schouwink, Gregory Stoclet, Christopher J.G. Plummer, Holger Frauenrath

Polymer 291 (2024) 126584

Contents lists available at ScienceDirect

Polymer

journal homepage: www.elsevier.com/locate/polymer

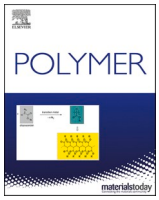

All-polyamide nanofibrillar composites by *in situ* fibrillation of aramid fibers

Nicolas Candau [a,b,1], Sylvain Galland [a,b], Oguzhan Oguz [a,b], Pascal Schouwink [c], Gregory Stoclet [d], Christopher J.G. Plummer [a,*], Holger Frauenrath [a,**]

[a] *Laboratory of Macromolecular and Organic Materials (LMOM), Institute of Materials (IMX), École Polytechnique Fédérale de Lausanne (EPFL), Station 12, 1015, Lausanne, Switzerland*

[b] *Laboratory for Processing of Advanced Composites (LPAC), Institute of Materials (IMX), École Polytechnique Fédérale de Lausanne (EPFL), Station 12, 1015, Lausanne, Switzerland*

[c] *ISIC Valais, École Polytechnique Fédérale de Lausanne (EPFL), Rue de l'industrie 17, CH-1951, Sion, Switzerland*

[d] *Unité Matériaux et Transformations (UMET), UMR CNRS 8207, Université de Lille Nord de France, USTL-ENSCL, Bat C7, BP 90108, 59652, Villeneuve d'Ascq, France*

ARTICLE INFO

Keywords:
Nanofibrillar composites
Polyamide 6,10
Nylon 6,10
Aramid
poly(*p*-phenylene terephthalamide)
Extrusion compounding
Mechanical properties

ABSTRACT

All-polyamide composites containing up to 30 *vol%* highly dispersed PPTA nanofibrils with diameters in the range 50–500 nm were prepared by melt-compounding polyamide 6,10 (PA610) with chopped poly(*p*-phenylene terephthalamide) (PPTA) fibers in the temperature range 260–300 °C using a twin-screw extruder. Injection moldings prepared from these composites showed not only large increases in tensile strength with respect to the unmodified PA610 matrix at temperatures well below the matrix melting point but also significant increases in melt elasticity. The melt elasticity was further enhanced by high-temperature heat treatments under quiescent conditions. It is suggested that the implied interfacial reinforcement may involve transamidation, which is known to occur extensively in polyamide melts.

1. Introduction

Glass and carbon fiber-reinforced plastic components are widely employed in lightweight structures, notably in the aerospace and automotive industries, thanks in large part to their high specific strength and stiffness, corrosion resistance, ease of processing, and design flexibility [1]. Thermoplastics reinforced with high-performance organic fibers composed of ultra-oriented rigid-chain polymers, such as poly(*p*-phenylene terephthalamide) (PPTA), may combine many of the benefits of conventional glass or carbon fiber-reinforced plastics with additional advantages, such as improved damage tolerance and reduced density [2]. However, PPTA fibers adhere poorly to most thermoplastics [3,4], and their low resistance to cleavage along the fiber axis severely limits their compressive strength [5]. Moreover, excessive mechanical degradation during melt processing of short PPTA fiber-reinforced composites may lead to far less reinforcement than would be expected for the virgin fibers based on standard micromechanical models [6].

The tendency of ultra-oriented rigid-chain polymer fibers to cleave along their axes is nevertheless exploited in the use of mechanical milling to produce microfibrillar materials from, e.g., aromatic polyamides or cellulose. These materials typically contain a significant proportion of "nanofibrils" with diameters as low as 10–100 nm, which have enormous potential as reinforcing elements thanks to not only their high specific axial stiffness and strength, but also their ultra-high aspect ratios compared with the parent fibers [7,8]. Microfibrillar PPTA produced in this way, commonly referred to as PPTA pulp, is hence highly effective in improving the abrasion resistance, toughness, and strength of thermoplastics and elastomers, provided the fibrils are adequately dispersed [9,10]. However, the high specific surface areas and strong interfibrillar interactions associated with microfibrillar materials make them difficult to disperse using conventional mixing techniques in polymer matrices with which they are weakly compatible. Model

* Corresponding author.
** Corresponding author.
E-mail addresses: christopher.plummer@epfl.ch (C.J.G. Plummer), holger.frauenrath@epfl.ch (H. Frauenrath).
[1] Present address: Departament de Ciència i Enginyeria de Materials (CEM), Escola d'Enginyeria Barcelona-Est (EEBE), Universitat Politècnica de Catalunya BarcelonaTech (UPC), Av. Eduard Maristany 16, 08019 Barcelona, Spain.

https://doi.org/10.1016/j.polymer.2023.126584
Received 26 September 2023; Received in revised form 2 December 2023; Accepted 10 December 2023
Available online 16 December 2023

systems based on pre-formed micro-/nanofibrils are hence often prepared using *ad hoc* techniques involving surface modification and/or solvent-aided dispersion, resulting in networks of highly interconnected curvilinear inclusions in the resulting nanocomposites [11]. In the case of PPTA pulp, dispersion is facilitated by using compatibilizers that react with free amine groups at the fibril surfaces generated by hydrolysis, plasma treatment, fluorination, or oxyfluorination [12]. However, such treatments are costly and may cause unacceptable degradation of the fibril properties [13]. It is consequently of particular interest to combine unmodified PPTA pulp with chemically similar thermoplastic polyamide matrices with which it has stronger intrinsic interfacial interactions [14–16], but the emphasis has so far been on polyamides with relatively low PPTA pulp contents and improvements in tribological properties [17,18].

An alternative route to microfibrillar polymer-polymer composites is to generate the reinforcing elements *in situ* by "converting instead of adding" them [19]. This may be achieved, e.g., by flow-induced elongation and orientation of a low viscosity minority component of an immiscible blend, as in the preparation of microfibrillar polystyrene-polyamide 6 composites by reactive extrusion of polystyrene blended with ε-caprolactam, which forms polyamide 6 *in situ* by anionic ring-opening polymerization (AROP) [20]. Indeed, AROP of lactams and its variants have also been used to produce a range of all-polyamide and single-polyamide composites [21–23]. In the case of thermoplastic polyamide and polyester blends, transamidation and transesterification reactions between the different components are expected to play an important role in the stabilization of the final morphology [24,25]. Transamidation catalysts have also been shown to improve the properties of all-polyamide composites prepared from pre-formed reinforcing elements that remain at least partly solid during processing [26]. Rapid, extensive transamidation is nevertheless known to take place without the need for catalysts during extrusion compounding of aliphatic polyamides with compatible semiaromatic copolyamides at sufficiently high temperatures [27], leading to homogeneous terpolymers with unique combinations of strength, stiffness, and ductility [28,29]. Moreover, it has been recently demonstrated that transamidation may lead to covalent bonding between aminopropyl-functionalized poly(dimethylsiloxane) and a solid semiaromatic polyamide (poly(hexamethylene terephthalamide-co-isophthalamide) substrate [30]. It follows that transamidation during high-temperature extrusion compounding of aliphatic polyamides and solid fibers composed of fully aromatic polyamides such as PPTA, may contribute significantly to interfacial interactions, particularly if it is accompanied by mechanical break-up of the fibers. PPTA fibers are widely considered to consist of bundles of aligned crystalline nanofibrils with high degrees of axial molecular orientation [31–34], separated in the lateral and axial directions by less ordered regions containing defects that may originate from chemical impurities or local concentrations of chain ends and constitute some 20–25 % of the total fiber volume [31–36]. If transamidation does occur at the PPTA-matrix interface, it is expected to be substantially accelerated if the mobile functional groups associated with such regions are exposed to the reactive melt [35,36].

Here we provide an account of the morphology and mechanical properties of well-dispersed, all-polyamide, nanofibrillar composites prepared by mechanical break-up and dispersion of unmodified, chopped PPTA fibers in an aliphatic polyamide, poly(hexamethylene sebacamide), also known as polyamide 6,10 (PA610), *in situ* during high-temperature extrusion compounding (Fig. 1), an approach that has been used recently to prepare cellulose-based fibrillar biocomposites [37]. Injection moldings of the present all-polyamide composites show large increases in tensile strength in the sold state, and significant melt elasticity at test temperatures above the melting point of the unmodified PA610 matrix, which point to the formation of a mechanically percolating network of PPTA fibrils. Moreover, the melt elasticity is reinforced by prolonged exposure to elevated temperatures in the quiescent state, suggesting enhanced interactions between the PPTA fibrils and/or the PPTA and the matrix, possibly involving transamidation, which may consequently also contribute to stabilization of the PPTA dispersion during compounding. High-temperature extrusion compounding of polyamides with high-melting point polyamide fibers is hence shown to be a straightforward route to lightweight, heat-resistant, melt-processable nanofibrillar composites with significantly enhanced tensile properties compared with the unmodified matrix.

2. Experimental

2.1. Melt compounding of polyamide composites

The polyamides used in this work were provided by EMS Chemie AG and stored under vacuum for at least 48 h before processing. PA610 (number average molecular weight, M_n = 16′000, weight average molecular weight, M_w = 32′000) was melt compounded with chopped PPTA fibers of initial length 6 mm and diameter 12 μm in a co-rotating twin-

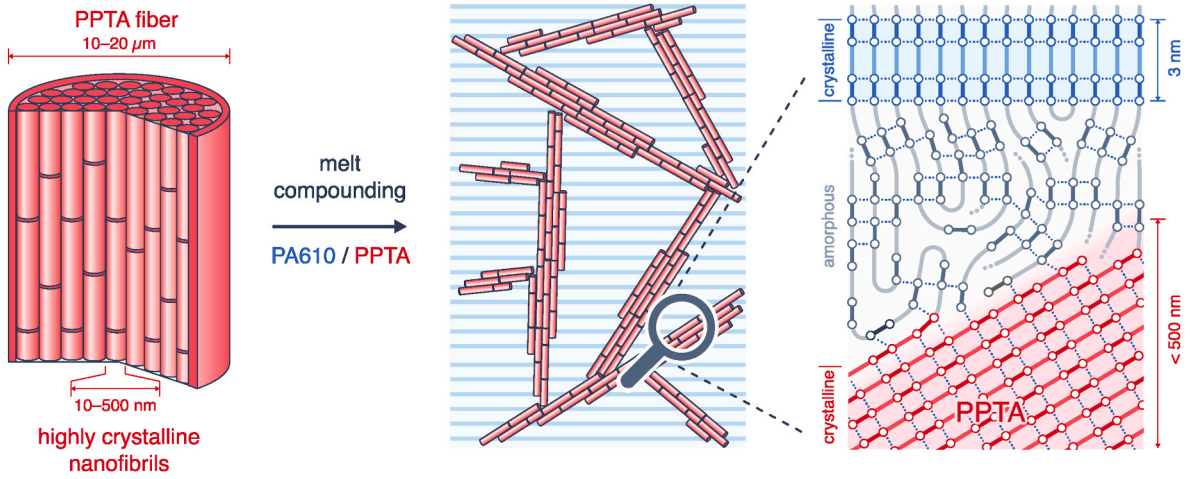

Fig. 1. *a)* Poly(*p*-phenylene terephthalamide (PPTA) fibers are widely considered to consist of bundles of aligned crystalline nanofibrils with high degrees of axial molecular orientation [31–34]. These are separated in the lateral and axial directions by less ordered regions containing defects that may originate from chemical impurities or local concentrations of chain ends and constitute some 20–25 % of the total fiber volume [31–36]. *b)* The PPTA fibers break up to form a network of nanofibrils *in situ* during melt-compounding with an aliphatic thermoplastic polyamide, poly(hexamethylene sebacamide) (PA610). *c)* Increased specific physical and chemical interfacial interactions, including covalent bond formation via transamidation, may contribute to increases in melt elasticity observed after high-temperature heat treatments, and hence to stabilization of the fibril dispersion in the polyamide matrix during compounding.

screw micro-compounder (DSM Micro 5), equipped with a back-flow channel to permit control of the residence time. The barrel temperature was set to between 260 and 300 °C, as required, and the polymer and fibers were compounded for various times at a screw speed of 100 rpm. The molten extrudate was then transferred directly to a DSM micro-injection molding machine and injection molded to give dog bone-shaped tensile test bars with gauge dimensions 2 × 4 × 30 mm^3 (thickness × width × length). The cylinder and mold temperatures were 260 and 130 °C, respectively, and the injection pressure was 6 bars. The test bars were dried under vacuum for 1 h at 180 °C (well above the matrix glass transition temperature, T_g, which is about 50 °C for dry PA610) and stored at room temperature under vacuum before further testing and analysis.

2.2. Mechanical testing (UTS)

The tensile test bars were tested using a universal testing machine (Walter + Bai UTM) at a nominal strain rate of 10 %/min. The strain was measured using a clip-on extensometer over an initial specimen length of 20 mm. A minimum of 5 specimens were tested for each composition and set of processing conditions. The Young's modulus was determined from the slope of the nominal stress-strain curve in the linear elastic regime, i.e., at strains below 1 %.

2.3. Differential scanning calorimetry (DSC)

DSC measurements (TA Instruments Q100) were performed under nitrogen (50 mL/min) using specimen masses of about 5 mg and a scanning rate of 10 °C/min. The melting point, T_m, was taken to be the temperature corresponding to the maximum in the melting endotherm, and the crystallization temperature, T_c, was taken to be the temperature corresponding to the maximum in the crystallization exotherm observed during cooling from temperatures above T_m.

2.4. Dynamic mechanical analysis (DMA)

The dynamic mechanical properties were characterized using a dynamic mechanical analyzer (DMA, Q800 TA Instruments) in tensile mode on injection molded rectangular test bars with approximate dimensions 1 × 2 × 10 mm^3 (thickness × width × length). The measurements were performed in the linear viscoelastic regime at a constant frequency of 1 Hz in the temperature range 25–110 °C with a heating rate of 3 °C/min.

2.5. Heat deflection temperature (HDT)

The heat deflection temperature (HDT) was defined as the temperature at which a loading-point deflection of 0.3 mm was observed at a flexural stress of 0.455 MPa in three-point bend tests on rectangular test bars with approximate dimensions 2 × 4 × 75 mm^3 (thickness × width × length) machined from the injection molded tensile test bars. The three-point bend tests were carried out using the same dynamic mechanical analyzer as for the DMA measurements, with the specimen in the flat-on position, and roller supports with a span of 50 mm. The temperature was increased from room temperature to 450 °C at 3 °C/min. The HDT defined in this way was therefore consistent with ISO 75 Method B, with the deflection adjusted to compensate the non-standard specimen geometry used here.

2.6. Small- and wide-angle X-ray scattering (SAXS/WAXS)

2D small-angle X-ray scattering (SAXS) and wide-angle X-ray scattering (WAXS) measurements were performed with a Xeuss 2.0 instrument (Xenocs) using Cu K_α radiation (wavelength, $\lambda = 1.5406$ Å) and point collimation. The sample to detector distance, which was about 18 cm for WAXS and 150 cm for SAXS, was calibrated using silver behenate as a standard. The data were recorded in transmission mode with a beam area of 500 × 500 μm^2 and a 2D Pilatus 200k detector, and standard corrections were applied prior to analysis. The intensity profiles were obtained by azimuthal integration of the 2D patterns using the fit2D software. The crystalline and amorphous contributions to the WAXS patterns were deconvoluted using Lorentzian and Gaussian functions respectively, while broad Bragg peaks observed at small angles were assumed to be due to the quasi-periodic stacking of alternating crystalline and amorphous lamellae.

WAXS data at different temperatures were obtained using a Panalytical Empyrean diffractometer equipped with a Pixcel 1D detector and chopped specimens loaded into a 1 mm Quartz capillary, which was rotated during data collection. The initial measurements at 30 and 50 °C resulted in comparatively high intensities because they were carried out with a 10 mm beam mask. However, the mask size was reduced to about 7 mm for measurements at and above 75 °C using lead tape, to ensure that the signal originated from well within the heated area of the specimen, assumed to be commensurate with the diameter of the modified nozzle of the Leister heat blower used to control the temperature (about 10 mm). The measurements were performed in steps of 0.055° with a total acquisition time of 25 min per pattern in the 2θ range 8–32°.

Crystallographic textures were characterized using the Herman's orientation function [38,39],

$$\langle P_2 \rangle = \frac{1}{2}\left(3\langle \cos^2 \varphi \rangle - 1\right), \tag{1}$$

the average value of the second order Legendre polynomial in $\cos\varphi$, where φ is the angle between a given diffraction plane normal and the fiber axis. $\langle P_2 \rangle = 1$ for perfect alignment of the plane normal with the fiber axis, $\langle P_2 \rangle = 0$ for random orientation, and $\langle P_2 \rangle = -0.5$ if the plane normals are randomly oriented in the plane perpendicular to the fiber axis. For a semicrystalline specimen with a transversely isotropic crystallographic texture, $\langle P_2 \rangle_{hkl}$ may be obtained from the variation in intensity with azimuthal scattering angle, χ, of the corresponding Debye ring in a two-dimensional WAXS pattern with the X-ray beam perpendicular to the fiber axis, using [38]

$$\langle P_2 \rangle_{hkl} = \frac{1}{2}\left(3\frac{\int_0^{\pi/2} I_{hkl}(\chi)\cos^2\chi \sin\chi d\chi}{\int_0^{\pi/2} I_{hkl}(\chi)\sin\chi d\chi} - 1\right) \tag{2}$$

2.7. Scanning electron microscopy (SEM)

Fracture surfaces from tensile specimens were observed using a Zeiss GeminiSEM 300 electron scanning microscope (SEM) equipped with a field emission gun and an in-lens detector. The acceleration voltage was 3 kV and specimens were coated with carbon to prevent excessive charging during electron irradiation.

2.8. Transmission electron microscopy (TEM)

200 nm thick longitudinal and cross sections were prepared from the dog bone-shaped specimens at −50 °C with a cutting speed of 1 s^{-1} using a Leica Microsystems EM UC7/FC7 Cryo-ultra-microtome equipped with a Diatome diamond knife. The sections were picked up on carbon covered copper grids, briefly heat treated at about 200 °C under nitrogen in a differential scanning calorimetry (DSC) cell to enhance the mass-thickness contrast, and observed in bright field using a Talos F200S G2 (ThermoFischer Scientific) transmission electron microscope (TEM) with an accelerating voltage of 200 kV.

3. Results and discussion

3.1. Morphology

PA610 was melt compounded with PPTA fibers at temperatures well

above the PA610 melting point, T_m, which is typically 225–230 °C, depending on its thermal history. In contrast with the brittle failure of glass or carbon fibers subject to high shear forces during extrusion [40], the PPTA fibers not only broke up into shorter lengths after short residence times under these conditions, but also cleaved parallel to their axes to form high-aspect-ratio fibrils with sub-micron diameters (Fig. 2, Fig. 3, Figure S1) [6,31–34]. The volume fraction of fibrillated material was estimated from the area fraction of the remaining un-fibrillated fiber fragments, which were clearly distinguishable in optical micrographs (Fig. 2). The volume fraction of fibrillated material increased with increasing residence time in the extruder for a given barrel temperature, decreased slightly for a given residence time as the extrusion temperature was increased from 260 to 300 °C, and increased with increasing PPTA fiber content under fixed extrusion conditions. These trends may be attributed to increased shear forces on the fibers at high PPTA contents and reduced extrusion temperatures [37]. At PPTA contents below 15 *vol%,* the fibers broke up into lengths of the order of 50 μm with diameters generally comparable with the initial fiber diameter, although some fibrillated material was visible in tensile fracture surfaces (Fig. 2*a,b*). However, as the PPTA content was increased to 22.5 *vol%* or more, the degree of fibrillation approached 90 *vol%* after a residence time of 10 min at 280 °C, and the fibrillated material was homogeneously dispersed in the PA610 matrix (Fig. 2*c*). Dissolution of the PA610 in formic acid confirmed the fibrils and any remaining un-fibrillated PPTA fragments to form a continuous self-supporting network at PPTA under these conditions (Fig. 2*d,e*).

Transmission electron microscopy (TEM) of heat-treated ultrathin cross-sections from the moldings showed the fibril diameters to be in the range 50–500 nm, i.e., a predominantly nanofibrillar morphology (Fig. 3). The number average circle-equivalent diameters of the fibril cross-sections were estimated from the TEM micrographs to be 256, 218 and 238 nm for 7.5, 15 and 22.5 *vol%* PPTA, respectively. The corresponding area-weighted diameters were 363, 350 and 475 nm, suggesting the dispersity of the fibrils to increase somewhat at the highest PPTA volume fraction, but the morphology otherwise to remain stable under the processing conditions in question.

TEM micrographs from specimens with low fibril volume fractions (Fig. 3*b*) also indicated the PA610 lamellae to radiate from the surfaces of the nanofibrils, consistent with observations of enhanced nucleation at the fiber surfaces in conventional PPTA-reinforced polyamides

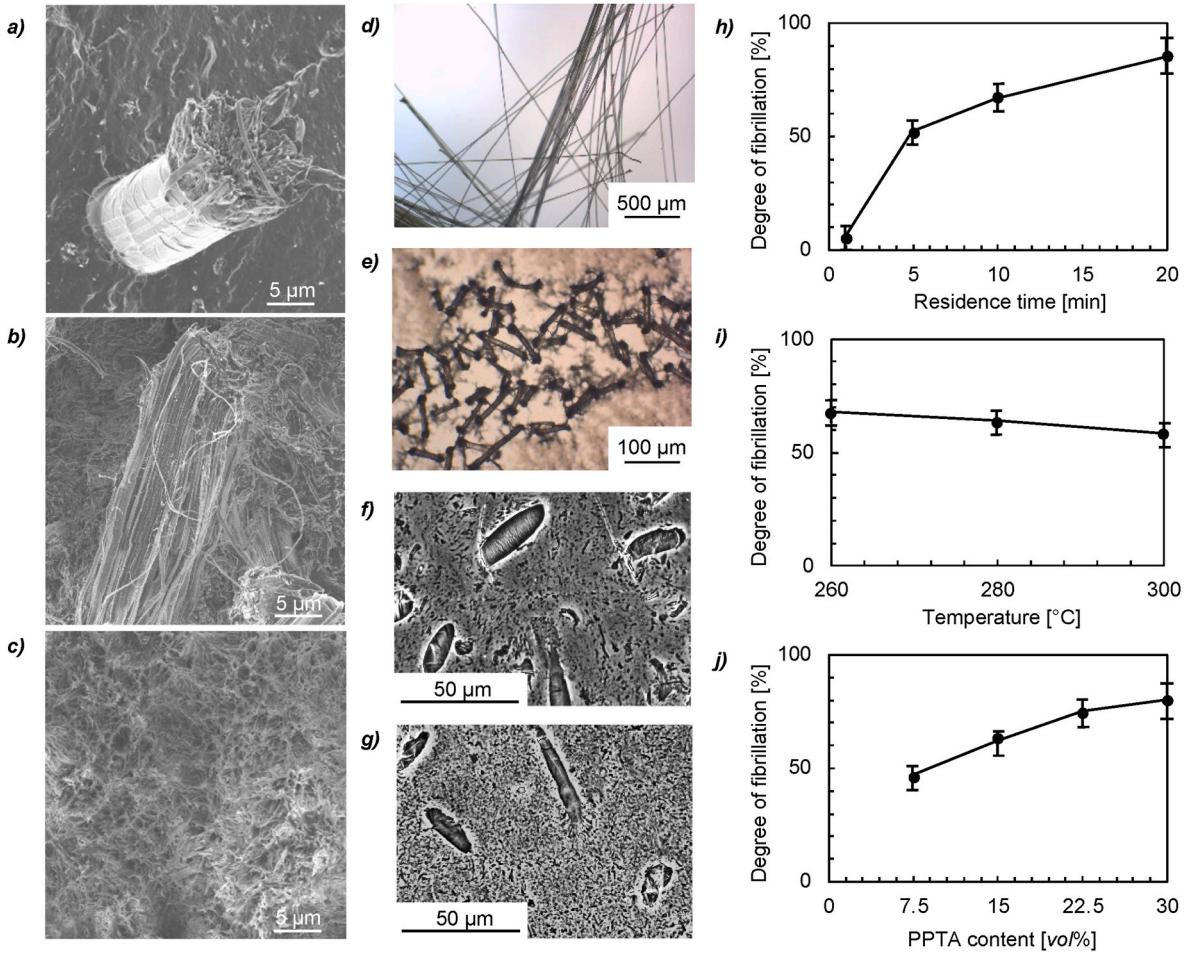

Fig. 2. *a-c)* Scanning electron microscopy (SEM) micrographs of room temperature tensile fracture surfaces (strain rate 10 %/min) from injection moldings of *a)* PA610–7.5 *vol*% PPTA, *b)* PA610-15 *vol*% PPTA and *c)* PA610–22.5 *vol*% PPTA extrusion compounded at 280 °C for 10 min. *d,e)* Bright field transmitted light optical micrograph (OM) of *d)* the as-received chopped PPTA fibers and e*)* the continuous network obtained after dissolution in formic acid of the PA610 matrix of PA610-15 *vol%* PPTA extrusion compounded at 280 °C for 10 min. *f,g)* Phase contrast transmitted light OM of microtomed sections from injection moldings of PA610-15 *vol %* PPTA extrusion compounded at 280 °C for *f)* 5 min and *g)* 20 min, containing approximately 7.5 and 10 *vol%* fibrillated PPTA, respectively. *h-j)* Degree of fibrillation as a function of *h)* residence time during extrusion compounding of PA610-15 *vol%* PPTA at 260 °C, *i)* temperature for PA610-15 *vol%* PPTA extrusion compounded for 10 min, and *j)* PPTA volume fraction for PA610-PPTA extrusion compounded for 10 min at 280 °C. The degree of fibrillation of the PPTA is defined as $(1 - f_{comp})/f_{init}$, where f_{init} is the nominal PPTA volume fraction and f_{comp} is the volume fraction of un-fibrillated PPTA after extrusion compounding, estimated from reflected light OM of internal surfaces from the moldings prepared by ultramicrotomy that intercepted at least 20 un-fibrillated PPTA fiber fragments. The experimental error was estimated by comparing measurements from different regions of selected specimens.

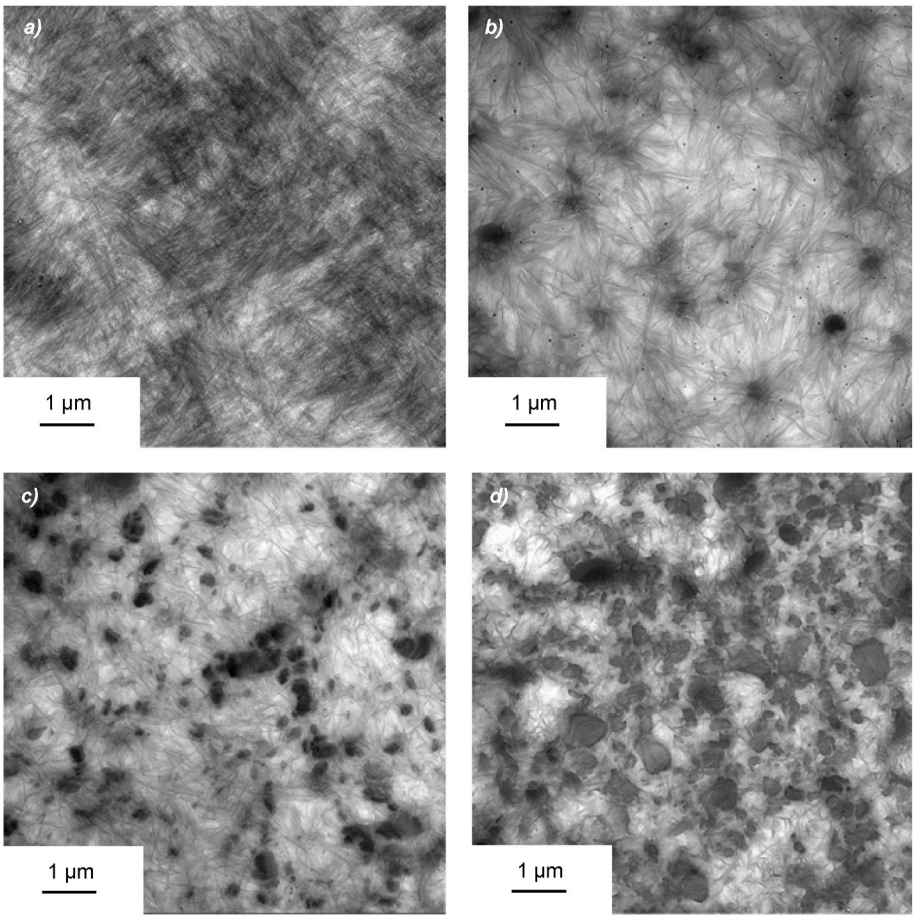

Fig. 3. TEM images of heat-treated ultrathin cross-sections taken transverse to the axis of injection moldings of *a)* PA610, *b)* PA610–7.5 *vol%* PPTA, *c)* PA610-15 *vol %* PPTA and *d)* PA610–22.5 *vol%* PPTA extrusion compounded at 260 °C for 10 min showing fibrillation and extensive matrix transcrystallinity in the presence of the PPTA.

[41–44], as well as other types of all-polyamide composite [22], so that the resulting transcrystalline layers impinged under the present processing conditions. The nucleating effect of the PPTA fibrils on the crystallization kinetics of the bulk specimens was reflected by: (i) increases in T_c, the peak temperature of the PA610 crystallization exotherm in differential scanning calorimetry (DSC) cooling scans at 10 °C/min, and increases in the degrees of crystallinity, χ, of the PA610, estimated from the enthalpy of crystallization, assuming a value of 197 J/g for fully crystalline PA610 [45] (Fig. 4*a*); (ii) decreases in the crystallization half-time, $\tau_{1/2}$, during isothermal crystallization from the melt (Fig. 4*b*). However, there was little further evolution in T_c and χ at PPTA contents beyond 15 *vol%*, implying the nucleating effect to saturate in this composition range for high degrees of fibrillation. Moreover, lower χ and T_c were observed for short residence times and reduced degrees of fibrillation at fixed PPTA content (Figure S2), confirming nucleation to be strongly dependent on break-up of the PPTA fibers.

Wide-angle X-ray diffraction (WAXD) indicated the dominant crystalline phase in the PA610 matrix to be the usual triclinic α-structure, comprising sheets of hydrogen-bonded chains in the all-*trans* conformation aligned with the *c*-axis, with the sheets stacked normal to the (010) planes in the standard representation of the unit cell [46]. A reversible Brill transition was also observed as the temperature increased from 23 °C to T_m, marked by convergence of the d_{100} and $d_{010/110}$ peaks (Fig. 4*c,d*, Figure S3), a phenomenon usually ascribed to conformational disorder of the crystalline aliphatic segments [47]. Once the PA610 had melted, Bragg peaks associated with the monoclinic structure of the PPTA fibrils could be resolved unambiguously at temperatures up to the onset of their decomposition at 500–580 °C [48] (Figure S4). The corresponding d_{hk0} spacings increased somewhat with further increases in temperature owing to thermal expansion [49], and there was also a small increase in the PPTA crystallinity index (Fig. 4*d*), defined as the ratio of the deconvoluted PPTA crystalline peak areas to the total area under the WAXD pattern (Figure S5), consistent with the increase in PPTA crystal perfection widely observed during high-temperature heat treatments [50]. The implied thermal stability of the microfibrillar PPTA was hence considerably greater than that of many ultra-oriented microfibrillar organic reinforcements currently used to modify the elastic properties of polymers in the glassy and rubbery states, including thermotropic liquid crystalline polymers, which typically soften at around 250 °C [51], and various forms of cellulose, which decompose at temperatures above about 230 °C [52]. The PA610 matrix was also found to undergo only minor mass loss at temperatures up to about 400 °C, suggesting there to be little effective degradation during processing (Fig. 4*c*). Indeed, PA610 has been shown previously to conserve its initial molar mass distribution during prolonged extrusion at temperatures of up to 330 °C despite the onset of rapid transamidation in this temperature range [27].

TEM images of transverse and longitudinal sections from the injection moldings showed preferential orientation of the PPTA fibrils along the specimen axes at all PPTA contents, although the fibrils adopted curvilinear trajectories at the μm scale (Fig. 5*a*). This orientation could not be quantified by 2D-WAXD because *in situ* measurements were not possible in the temperature range where the main PPTA Bragg reflections were clearly visible. However, equatorial, or near-equatorial maxima in the intensity of the PA610 (100) reflections were observed at 21 °C, while the intensity of the corresponding (002) reflections

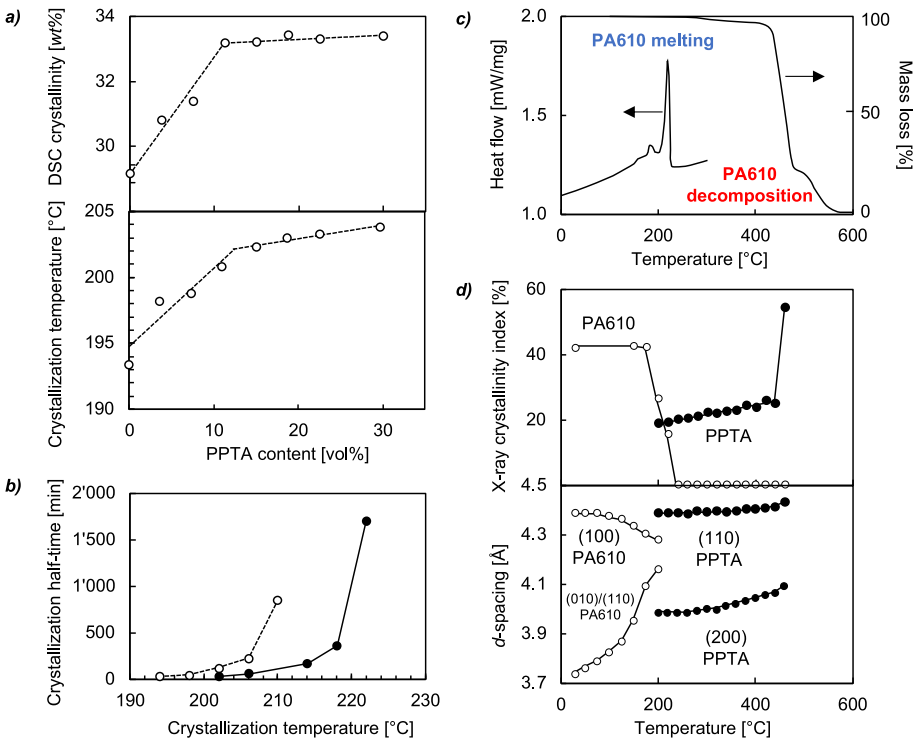

Fig. 4. *a)* Crystallization temperature and degree of crystallinity of the PA610 from DSC cooling scans at 10 °C/min as a function of PPTA content. *b)* Crystallization half-times, $\tau_{1/2}$, during isothermal crystallization from the melt for PA610 and PA610-15 *vol%* PPTA. *c)* DSC heating scan at 10 °C/min from PA610-15 *vol%* PPTA and thermogravimetric analysis (TGA) mass loss from PA610-15 *vol%* PPTA, indicating matrix decomposition from about 400 °C and decomposition of the PPTA from 500 °C. *d)* WAXD crystallinity index and PA610 and PPTA *d*-spacings in PA610-15 *vol%* PPTA as a function of temperature. All the specimens were extrusion compounded at 260 °C for 10 min, and examples of the deconvolution of the WAXD peaks are given in Figure S5.

reached a maximum in the meridional or near-meridional positions (Fig. 5*b*, Figure S6). There was hence preferential orientation of the *c**-axes of the PA610 reciprocal lattice along the specimen axes, and transverse orientation of the *a**-axes, which correspond roughly to the lamellar trajectories [53]. Similarly, 2D-SAXS patterns showed marked meridional scattering associated with the lamellar long period, confirming the lamellae to be preferentially oriented transverse to the specimen axes (Fig. 5*c*, Figure S7), consistent with the observed preferential alignment of the PPTA parallel to the flow direction and the observed matrix transcrystallinity. The extent of this orientation nevertheless remained modest at all PPTA contents, as reflected by the Herman's orientation functions, $\langle P_2 \rangle_{002}$ and $\langle P_2 \rangle_{100}$ (Fig. 5*d*) [38,39].

3.2. Mechanical properties

In the absence of PPTA, the tensile storage modulus, E', obtained from dynamic mechanical analysis (DMA) heating scans of the PA610 injection moldings showed a low-temperature glassy plateau at approximately 1.9 GPa and then decreased by about an order of magnitude in the glass transition zone, which was centered on 70 °C. A second plateau, corresponding to the "rubbery" regime, extended from the glass transition zone up to the melting transition at around 225 °C, beyond which E' was too small to be measured (Fig. 6*a*). As expected, the presence of the fibrillated PPTA led to global stiffness reinforcement consistent with those reported previously for cellulose-based nanofibrillar composites with comparable degrees of dispersion [52,54]. However, while E' measured at 21 °C increased from 1.9 to only about 2.5 GPa between 0 and 15 *vol%* PPTA, it nearly doubled as the PPTA content was increased further to 30 *vol%* (Fig. 6*b*). Moreover, E' well in excess of 1 MPa were observed at temperatures above T_m for PPTA contents of 15 *vol%* or more. Indeed, E' increased substantially in this composition range on heating at 3 °C/min from about 240 to 400 °C, this latter temperature corresponding to the onset of significant matrix degradation according to the TGA measurements (Fig. 4c).

Given the absence of large increases in the matrix or fiber orientation with PPTA content in the range considered, the enhanced stiffness reinforcement observed at PPTA contents above 15 *vol%* was attributed to increased fibrillation (Fig. 2) and the establishment of a load-bearing, mechanically-percolating network involving the PPTA fibrils. Stress transfer via such a network would imply break down of the usual assumption of constant stress conditions (the Reuss limit) in models for the low-strain elastic response of non-interacting curvilinear reinforcing elements [55], leading to an increase in stress at a given strain with respect to the predictions of such models. It would also account for the significant elasticity observed at temperatures well above T_m. The importance of percolating mechanical contacts for reinforcement has been demonstrated previously for solution-processed composites containing networks of nanofibrillar cellulose or highly exfoliated clay platelets, which are permanently disrupted by large deformations in the melt state, resulting in a substantial loss in stiffness [56,57]. In the present case, however, the putative network was formed *in situ* during melt extrusion and remained effective after injection molding, implying the fiber-fiber interactions to be reversible with respect to mechanical deformation at high temperatures.

The increases in E' with increasing PPTA content below T_m were reflected by similar increases in the quasi-static Young's moduli, E, determined from tensile tests. These were accompanied by substantial increases in tensile strength, i.e., the maximum nominal stress, σ_{max}, reached during the test, which were associated with a progressive decrease in the strain at failure, ε_{max}, in both the glassy and rubbery states (Fig. 7, Table 1). The improved tensile strength was a consequence of not only an increase in the yield stress, σ_y, but also the onset of marked strain-hardening beyond the yield stress as the PPTA content increased, so that the yield stress was no longer clearly defined at the highest PPTA contents. This again strongly suggested that the PPTA fibrils formed, or

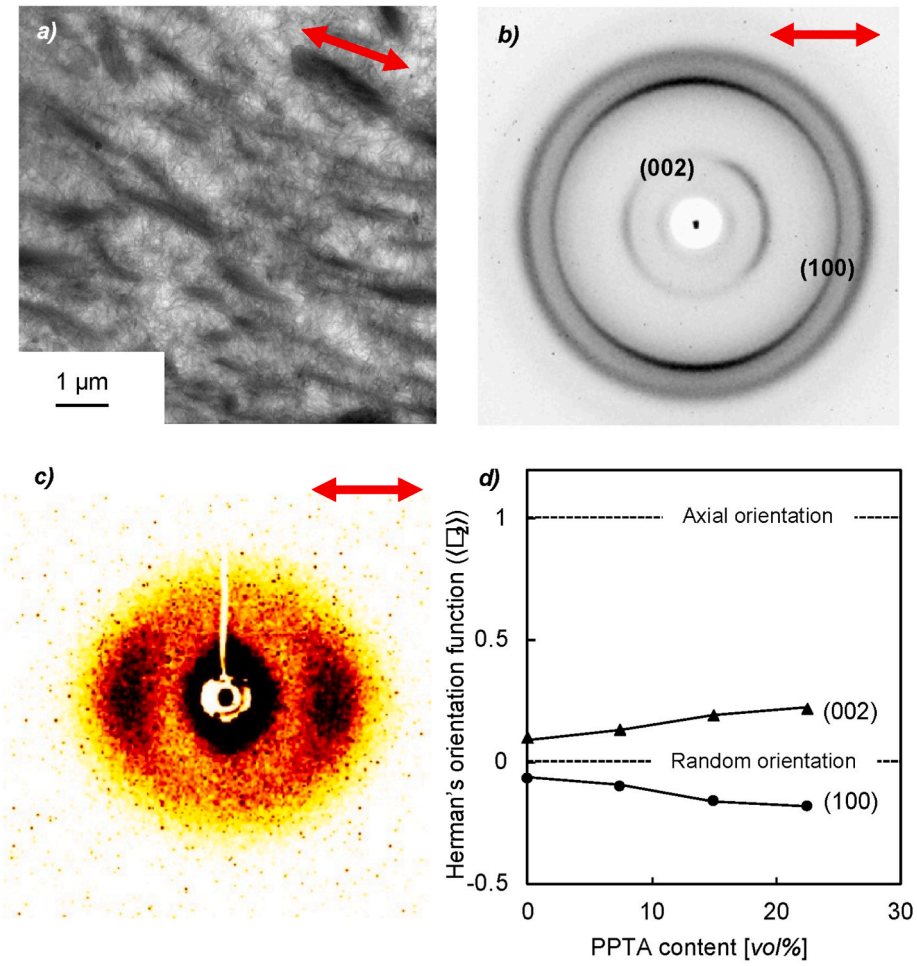

Fig. 5. *a)* TEM image of a thin section taken parallel to the axis of an injection molding of PA610-15 *vol%* PPTA extrusion compounded at 260 °C for 10 min, showing fibril orientation along the injection axis (cf. Fig. 3*c*). *b)* 2D-WAXD and *c)* 2D-SAXS patterns from PA610-15 *vol%* PPTA. The injection direction is indicated by the red arrow in each case. *d)* Herman's orientation functions $\langle P_2 \rangle_{002}$ and $\langle P_2 \rangle_{100}$ from injection moldings with the different PPTA contents extrusion compounded at 260 °C for 10 min showing preferential orientation of the (002) plane normals parallel to the specimen axis and of the (100) plane normals transverse to the specimen axis ($\langle P_2 \rangle = 1$ corresponds to perfect alignment parallel with the specimen axis and $\langle P_2 \rangle = -0.5$ corresponds to random alignment in the plane transverse to the specimen axis [38,39]). (For interpretation of the references to colour in this figure legend, the reader is referred to the Web version of this article.)

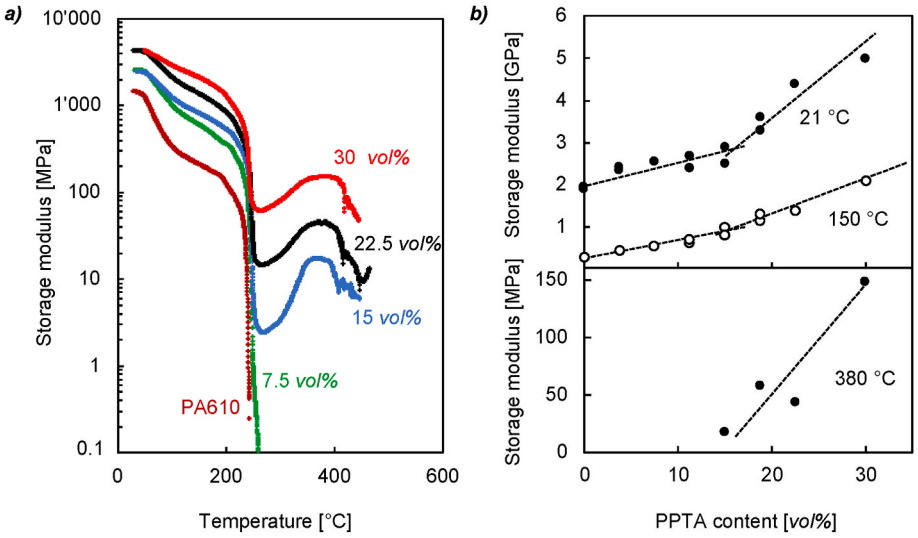

Fig. 6. *a)* Tensile storage modulus, *E'*, as a function of temperature from dynamic mechanical analysis (DMA) heating scans at a frequency of 1 Hz for the different PPTA contents indicated. *b) E'* as a function of PPTA content at temperatures of 23 °C (glassy), 150 °C (rubbery) and 380 °C (molten). All the results shown were obtained from injection moldings of composites extrusion compounded at 260 °C for 10 min.

participated in a mechanically percolating network at sufficiently high concentrations.

To investigate network formation further, representative microfibrillar composites containing 15 *vol%* PPTA and extrusion compounded at 260 °C for 10 min, were subjected to additional high-temperature heat treatments under conditions conducive to matrix transamidation in PA610. These treatments did not affect the dynamic response at temperatures up to the onset of PA610 melting at about 225 °C (Fig. 8*a*). However, at higher temperatures, a plateau in E' at close to 20 MPa was observed in the heat-treated composites, which extended up to the degradation temperature. This behavior contrasted with that of the un-heat-treated composites, in which E' fell to about 2 MPa before rising to 20 MPa as the temperature approached the matrix degradation temperature. Tensile tests on the same composites at 250 °C and a strain rate of 100 min^{-1} confirmed there to be significant elasticity above the melting point of the matrix, not only under dynamic loading but also up to large strains under quasi-static conditions (Fig. 8*b*). Moreover, the heat-treated composites showed a far higher tensile modulus in the tensile tests at 250 °C than the un-heat-treated composites, consistent with the DMA results, and a more than two-fold increase in tensile strength. However, their elongation at break remained close to that observed prior to heat treatment.

Because the high-temperature heat treatments took place under quiescent conditions, the corresponding reinforcement of the melt elasticity was inferred to be due to increased specific interactions and/or covalent bonding between the PPTA fibrils and/or the PPTA and the PA610 matrix, as opposed to further mechanical break-up or dispersion of the fibrils (the stiffness of the PPTA itself is not expected to change markedly even after prolonged heat treatment at 300 °C [50,58]). Moreover, the increases in E' with temperature above T_m observed in first DMA scans for nanofibrillar PPTA contents of 15 *vol%* or more were maintained on cooling to T_m and during subsequent heating and cooling cycles, and could also be reproduced by high-temperature heat treatment *in situ* in the DMA (Figure S8). It was not possible to establish here whether covalent bonding took place between the PA610 and the PPTA using direct analytical techniques. However, there is evidence from the literature for the formation of covalent bonds between aramids and aliphatic polyamides by transamidation in the melt state [59], and we have previously shown transamidation involving semiaromatic polyamides to occur rapidly not only under melt compounding conditions but also at solid polyamide surfaces in contact with an amide-functionalized melt [27,28,30]. Although the surfaces of as-spun PPTA fibers are generally considered to be poor in accessible functional groups, the internal interfaces from which fibrillation presumably originates are expected to contain very high concentrations of more reactive chain ends [31–34]. Indeed, improvements in the compressional strength have been reported for aramid fibers reinforced by using chemical treatments to partially break up their constituent fibrils, followed by crosslinking of the freshly exposed surfaces [60,61]. Mechanical exposure of the fibrils to a suitably reactive environment may therefore promote covalent bonding at the interfaces, which may in turn contribute to the formation of a stable fibril dispersion during compounding. Moreover, covalent bond formation due to transamidation should be reversible with respect to the large high-temperature shear deformations associated with extrusion and injection, and consequently not compromise processability [62].

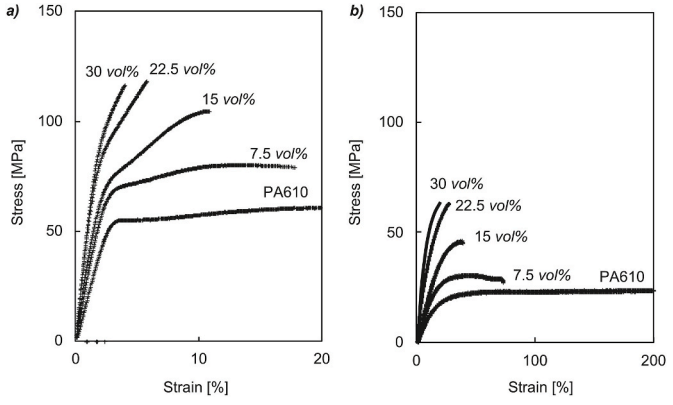

Fig. 7. Representative nominal tensile stress-strain curves from injection moldings of composites extrusion compounded at 260 °C for 10 min for the different PPTA contents indicated at *a)* 21 °C (glassy) and *b)* 150 °C (rubbery) and a nominal strain rate of 10 %/min.

Table 1
Young's modulus, E, nominal yield stress, σ_y, nominal tensile strength, σ_{max}, and strain at failure, ε_{max}, from tensile tests at 21 °C and a nominal strain rate of 10 %/min on injection moldings of composites extrusion compounded at 260 °C for 10 min for the different PPTA contents indicated. In the absence of a clear yield drop, the yield stress was taken to correspond to the knee in the stress-strain curves, i.e., the stress, σ, corresponding to the first point of inflection in $d\sigma/d\varepsilon$ plotted as a function of the nominal strain, ε.

PPTA [*vol%*]	E [GPa]	σ_y [MPa]	σ_{max} [MPa]	ε_{max} [%]
0	2.4 ± 0.1	55 ± 1	61 ± 1	76 ± 30
7.5	3.6 ± 0.1	69 ± 1	80 ± 1	18 ± 8
15	4.1 ± 0.1	72 ± 1	105 ± 1	11 ± 4
22.5	5.6 ± 0.1	79 ± 1	118 ± 1	5.8 ± 2
30	5.9 ± 0.1	85 ± 1	116 ± 1	4.0 ± 2

A further direct consequence of the presence of a robust elastic network in the composites at high temperatures was an increase in heat stability. This was evidenced by an increase in the heat deflection temperature (HDT) from about 180 °C for the unmodified PA610 matrix to over 220 °C for the as-molded composites containing 15 *vol%* PPTA. This latter HDT value is comparable to that of typical glass fiber-reinforced grades of PA610 as determined by ISO 75 Method B [63]. Moreover, whereas the unmodified PA610 underwent viscous flow when subject to a flexural stress of 0.455 MPa at temperatures above its T_m of about 225 °C, a maximum deflection of 16 mm was observed in PA610-15 *vol%* PPTA extruded at 260 °C for 10 min, which remained stable between T_m and the degradation temperature, despite extensive charring of the matrix (Fig. 8*c*). The maximum deflection decreased to about 10 mm in PA610-15 *vol%* PPTA extruded at 260 °C for 10 min and heat treated for 3 h at 300 °C. The heat stability was hence substantially improved with respect to polyamide-based composites based on nanocellulose, which show limited high-temperature elasticity, owing to both significant aggregation of the reinforcing fibers at concentrations greater than 10 *wt%*, and thermal degradation of the fibers themselves [64,65].

4. Conclusions

High-temperature extrusion compounding of commercial chopped PPTA fibers with a thermoplastic aliphatic polyamide is a straightforward and effective way of preparing well-dispersed, temperature-resistant, all-polyamide nanofibrillar PPTA-reinforced composites with fibril diameters ranging from 50 to 500 nm. Under the present compounding conditions, PPTA contents of 15 *vol%* or more led to substantial increases in stiffness and tensile strength. Thus, a Young's modulus and tensile strength of about 6 GPa and 115 MPa, respectively, were obtained for a PPTA content of 30 *vol%*. Although these values were approximately half those reported for PA610 reinforced with 30 *vol%* short E-glass fiber (GF) under ideal molding conditions [63], the corresponding density increase with respect to pure PA610 is significantly lower (around 10 % compared with 50 % for the GF-reinforced PA610).

These improvements are attributed to enhanced fibrillation and strong fibril-matrix interactions, resulting in the formation of a mechanically percolating PPTA network. It is also suggested that transamidation at the fibril-matrix interfaces may result in increased melt elasticity, as supported by heat treatment experiments, in which case it

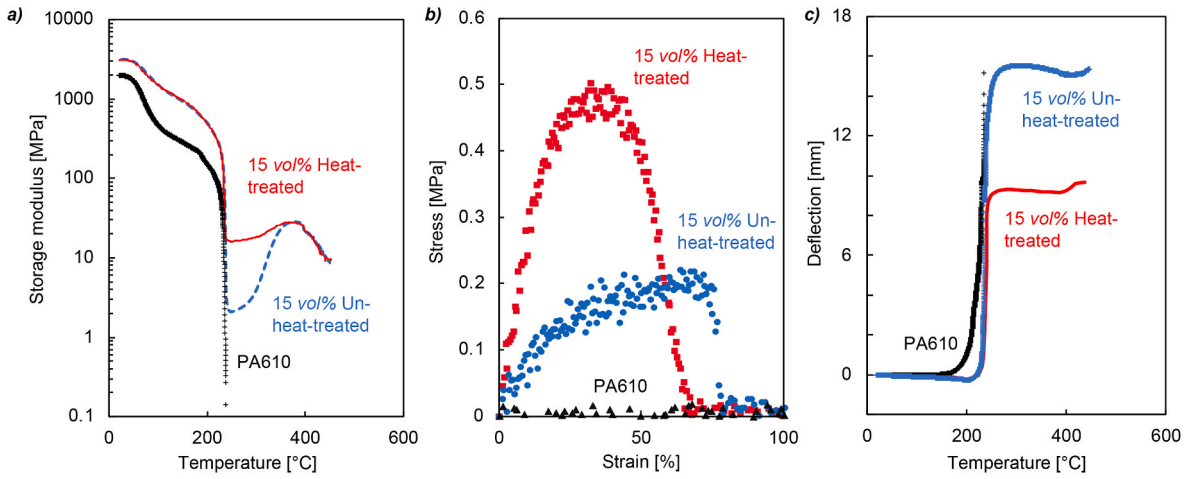

Fig. 8. *a)* Storage modulus, E', as a function of temperature from dynamic mechanical analysis heating scans at a frequency of 1 Hz for injection molded specimens of PA610, PA610-15 *vol%* PPTA extrusion compounded at 260 °C for 10 min ("Un-heat-treated"), and PA610-15 *vol%* PPTA extrusion compounded at 260 °C for 10 min and then heat treated for 3 h at 300 °C ("Heat-treated"). Heat treatment was carried out in a dog bone-shaped mold at a pressure of 200 bars using a hot press. *b)* Stress-strain curves from the same materials tested at 250 °C and a constant strain rate of 100 min^{-1}. *c)* Heat deflection test results for injection molded specimens of PA610 and PA610-15 *vol%* PPTA extrusion compounded at 260 °C for 10 min ("Un-heat-treated") and PA610-15 *vol%* PPTA extrusion compounded at 260 °C for 10 min and then heat treated for 3 h at 300 °C ("Heat-treated"). The specimens were loaded in three-point bending to an equivalent stress of 0.455 MPa using the same apparatus as for the DMA measurements in *a)* and *b)*.

may also contribute to stabilization of the fibril dispersion during compounding. In contrast, conventional short PPTA fiber-reinforced polyamides show only modest reinforcement, precisely because of the fiber break-up observed here in the early stages of extrusion compounding, which leads primarily to low-aspect-ratio PPTA fragments rather than fibrils [6].

This approach holds promise for the reinforcement of not only of PA610 but also a wide range of other aliphatic and semiaromatic polyamide thermoplastics. Such materials offer potential advantages over conventional short inorganic fiber-reinforced thermoplastics, including improved surface finish and weld-line strength, and reduced tool wear, and may consequently be of significant interest for the replacement of metals in structural applications requiring lightweight, heat-resistant parts. They also provide a foundation for the preparation of hybrid polyamide composites that combine fibrillated PPTA with other types of reinforcement, e.g., GF, which we are currently investigating for possible synergistic effects.

CRediT authorship contribution statement

Nicolas Candau: Formal analysis, Investigation, Methodology, Visualization, Writing – original draft, Writing – review & editing. **Sylvain Galland:** Investigation, Methodology. **Oguzhan Oguz:** Investigation. **Pascal Schouwink:** Investigation. **Gregory Stoclet:** Investigation. **Christopher J.G. Plummer:** Formal analysis, Funding acquisition, Investigation, Methodology, Supervision, Visualization, Writing – original draft, Writing – review & editing. **Holger Frauenrath:** Conceptualization, Funding acquisition, Methodology, Project administration, Supervision, Visualization, Writing – review & editing.

Declaration of competing interest

The authors declare that they have no known competing financial interests or personal relationships that could have appeared to influence the work reported in this paper.

Data availability

Data will be made available on request.

Acknowledgment

This work was supported by Innosuisse - Schweizerische Agentur für Innovationsförderung (project 15503.1 PFIW-IW). The Région Nord Pas-de-Calais and the European Regional Development Fund (FEDER) are acknowledged for funding and supporting the SAXS facility. The authors also thank the Interdisciplinary Electron Microscopy Center (CIME) of the EPFL for its technical assistance.

Appendix A. Supplementary data

Supplementary data to this article can be found online at https://doi.org/10.1016/j.polymer.2023.126584.

References

[1] S.-Y. Fu, B. Lauke, Y.-W. Mai, Science and Engineering of Short Fibre Reinforced Polymer Composites, Woodhead Publishing, Cambridge, 2009.
[2] H.G. Chae, S. Kumar, Rigid-rod polymeric fibers, J. Appl. Polym. Sci. 100 (2006) 791–802, https://doi.org/10.1002/app.22680.
[3] J. Kalantar, L.T. Drzal, The bonding mechanism of aramid fibres to epoxy matrices, J. Mater. Sci. 25 (1990) 4186–4193, https://doi.org/10.1007/BF00581071.
[4] D.B. Eagles, B.F. Blumentritt, S.L. Cooper, Interfacial properties of Kevlar-49 fiber-reinforced thermoplastics, J. Appl. Polym. Sci. 20 (1976) 435–448, https://doi.org/10.1002/app.1976.070200216.
[5] D. Tanner, J.A. Fitzgerald, B.R. Phillips, The kevlar story—an advanced materials case study, Angew Chem. Int. Ed. Engl. 28 (1989) 649–654, https://doi.org/10.1002/anie.198906491.
[6] Z. Yu, J. Brisson, A. Ait-Kadi, Prediction of mechanical properties of short kevlar fiber-nylon-6,6 composites, Polym. Compos. 15 (1994) 64–73, https://doi.org/10.1002/pc.750150110.
[7] A.F. Turbak, F.W. Snyder, K.R. Sandberg, Microfibrillated cellulose, a new cellulose product: properties, uses, and commercial potential, J. Appl. Polym. Sci. Appl. Polym. Symp. 37 (1983) 815–827.
[8] D.M. Haines, T.F. Schuler, Dispersible Aramid Pulp, 1992. US Patent 5171402A.
[9] J. Wu, X.H. Cheng, The tribological properties of Kevlar pulp reinforced epoxy composites under dry sliding and water lubricated condition, Wear 261 (2006) 1293–1297, https://doi.org/10.1016/j.wear.2006.03.014.
[10] W. Wu, Y. Zhou, L.Q. Zhang, Reinforcing mechanism of novel aramid pulp short fibre in chloroprene rubber matrix, Adv. Mater. Res. 11–12 (2006) 513–516. https://doi.org/10.4028/www.scientific.net/AMR.11-12.513.
[11] S. Thomas, K. Joseph, S.K. Malhotra, K. Goda, M.S. Sreekala, Polymer Composites, Macro- and Microcomposites, John Wiley & Sons, Chichester, 2012.
[12] M. Mukherjee, C.K. Das, A.P. Kharitonov, Fluorinated and oxyfluorinated short Kevlar fiber-reinforced ethylene propylene polymer, Polym. Compos. 27 (2006) 205–212, https://doi.org/10.1002/pc.20195.

[13] J. Yatvin, S.A. Sherman, S.F. Filocamo, J. Locklin, Direct functionalization of Kevlar® with copolymers containing sulfonyl nitrenes, Polym. Chem. 6 (2015) 3090–3097, https://doi.org/10.1039/C5PY00090D.

[14] D. Bhattacharyya, S. Fakirov, Synthetic Polymer-Polymer Composites, Carl Hanser Verlag, Munich, 2012.

[15] O.A. Khondker, T. Fukui, M. Inoda, A. Nakai, H. Hamada, Fabrication and mechanical properties of aramid/nylon plain knitted composites, Compos. Part Appl. Sci. Manuf. 35 (10) (Oct. 2004) 1195–1205, https://doi.org/10.1016/j.compositesa.2004.03.004.

[16] Z. Yu, A. Ait-Kadi, J. Brisson, Nylon/Kevlar composites. I: mechanical properties, Polym. Eng. Sci. 31 (1991) 1222–1227, https://doi.org/10.1002/pen.760311611.

[17] I. Faramarzi, M. Razzaghi-Kashani, Improvements in tribological properties of polyamide 6 by application of aramid pulp, Iran. Polym. J. (Engl. Ed.) 24 (2015) 329–335, https://doi.org/10.1007/s13726-015-0326-3.

[18] N. Rastegar, I. Faramarzi, M. Razzaghi-Kashani, Synergy in tribological properties of polyamide 6 containing aramid pulp and irradiated polytetrafluoroethylene hybrid additives, Iran. Polym. J. (Engl. Ed.) 30 (2021) 613–621, https://doi.org/10.1007/s13726-021-00917-w.

[19] S. Fakirov, Nano-/microfibrillar polymer–polymer and single polymer composites: the converting instead of adding concept, Compos. Sci. Technol. 89 (2013) 211–225, https://doi.org/10.1016/j.compscitech.2013.10.007.

[20] D. Yan, J. Li, J. Li, H. Liu, H. Zhou, G. Shen, Novel polyamide 6/polystyrene in situ microfibrillar blends prepared by anionic polymerization of ε-caprolactam via reactive extrusion, Macromol. Mater. Eng. 301 (2016) 1242–1247, https://doi.org/10.1002/mame.201600178.

[21] N. Dencheva, D.M. Vale, Z. Denchev, Dually reinforced all-polyamide laminate composites via microencapsulation strategy, Polym. Eng. Sci. 57 (2017) 806–820, https://doi.org/10.1002/pen.24456.

[22] N. Dencheva, Z. Denchev, A.S. Pouzada, A.S. Sampaio, A.M. Rocha, Structure–properties relationship in single polymer composites based on polyamide 6 prepared by in-mold anionic polymerization, J. Mater. Sci. 48 (2013) 7260–7273, https://doi.org/10.1007/s10853-013-7546-8.

[23] T. Ageyeva, I. Sibikin, J. Karger-Kocsis, Polymers and related composites via anionic ring-opening polymerization of lactams: recent developments and future trends, Polymers 10 (2018) 357, https://doi.org/10.3390/polym10040357, 2018.

[24] T. Sadik, F. Becquart, J.-C. Majesté, M. Taha, In-melt transesterification of poly (lactic acid) and poly(ethylene-co-vinylalcohol), Mater. Chem. Phys. 140 (2013) 559–569, https://doi.org/10.1016/j.matchemphys.2013.04.004.

[25] M. Vannini, P. Marchese, A. Celli, C. Lorenzetti, Block and random copolyamides of poly(m-xylylene adipamide) and poly(hexamethylene isophthalamide-co-terephthalamide): methods of preparation and relationships between molecular structure and phase behavior, Polym. Eng. Sci. 55 (2015) 1475–1484, https://doi.org/10.1002/pen.23994.

[26] D. Bhattacharyya, P. Maitrot, S. Fakirov, Polyamide 6 single polymer composites, Express Polym. Lett. 3 (2009) 525–532, https://doi.org/10.3144/expresspolymlett.2009.65.

[27] J. Cretenoud, S. Galland, C.J.G. Plummer, V. Michaud, A. Bayer, N. Lamberts, B. Hoffmann, H. Frauenrath, High-temperature copolyamides obtained by the efficient transamidation of crystalline–crystalline polyamide blends, J. Appl. Polym. Sci. 134 (2017), 44349, https://doi.org/10.1002/app.44349.

[28] N. Candau, S. Galland, J. Cretenoud, S. Balog, V. Michaud, J.-M. Chenal, O. Lame, C.J.G. Plummer, H. Frauenrath, High-performance polyamides with engineered disorder, Polym. Chem. 12 (2021) 6426–6435, https://doi.org/10.1039/d1py01225h.

[29] N. Candau, J.-M. Chenal, O. Lame, P. Schouwink, V. Michaud, C.J.G. Plummer, H. Frauenrath, Enhanced ductility in high performance polyamides due to strain-induced phase transitions, Polymer 238 (2022), 124424, https://doi.org/10.1016/j.polymer.2021.124424.

[30] M. Giffin, C.J.G. Plummer, Holger Frauenrath, Thermoplastic toughening of a semiaromatic polyamide with an amino-telechelic polyethylene, ACS Appl. Mater. Interfaces 15 (2023) 28430–28441, https://doi.org/10.1021/acsami.3c00599.

[31] R. Edmunds, M.A. Wadee, On kink banding in individual PPTA fibres, Compos. Sci. Technol. 65 (2005) 1284–1298, https://doi.org/10.1016/j.compscitech.2004.12.034.

[32] H.H. Yang, Kevlar Aramid Fiber, John Wiley & Sons, Chichester, 1993.

[33] R.J. Morgan, C.O. Pruneda, W.J. Steele, The relationship between the physical structure and the microscopic deformation and failure processes of poly(p-phenylene terephthalamide) fibers, J. Polym. Sci., Polym. Phys. Ed. 21 (1983) 1757–1783, https://doi.org/10.1002/pol.1983.180210913.

[34] M. Panar, P. Avakian, R.C. Blume, K.H. Gardner, T.D. Gierke, H.H. Yang, Morphology of poly(p-phenylene terephthalamide) fibers, J. Polym. Sci., Polym. Phys. Ed. 21 (1983) 1955–1969, https://doi.org/10.1002/pol.1983.180211006.

[35] S. Ran, X. Zong, D. Fang, B.S. Hsiao, B. Chu, P.M. Cunniff, R.A. Phillips, Studies of the mesophase development in polymeric fibers during deformation by synchrotron SAXS/WAXD, J. Mater. Sci. 36 (2001) 3071–3077, https://doi.org/10.1023/A:1017953412385.

[36] S. Ran, D. Fang, X. Zong, B.S. Hsiao, B. Chu, P.M. Cunniff, Structural changes during deformation of Kevlar fibers via on-line synchrotron SAXS/WAXD techniques, Polymer 42 (2001) 1601–1612, https://doi.org/10.1016/S0032-3861(00)00460-2.

[37] H. Taheri, M. Hietala, K. Oksman, One-step twin-screw extrusion process of cellulose fibers and hydroxyethyl cellulose to produce fibrillated cellulose biocomposite, Cellulose 27 (2020) 8105–8119, https://doi.org/10.1007/s10570-020-03287-3.

[38] G.R. Mitchell, A.H. Windle, The determination of molecular orientation in uniaxially compressed PMMA by X-ray scattering, Polymer 24 (1983) 285–290, https://doi.org/10.1016/0032-3861(83)90264-1.

[39] I.M. Ward, J. Sweeney, Mechanical Properties of Solid Polymers, John Wiley & Sons, 2012.

[40] S.-H. Wu, F.-Y. Wang, C.-C.M. Ma, W.-C. Chang, C.-T. Kuo, H.-C. Kuan, W.-J. Chen, Mechanical, thermal and morphological properties of glass fiber and carbon fiber reinforced polyamide-6 and polyamide-6/clay nanocomposites, Mater. Lett. 49 (2001) 327–333, https://doi.org/10.1016/S0167-577X(00)00394-3.

[41] Z. Yu, A. Ait-Kadi, J. Brisson, Nylon/Kevlar composites. II: investigation of interfaces, Polym. Eng. Sci. 31 (1991) 1228–1232, https://doi.org/10.1002/pen.760311612.

[42] C. He, X. Dong, X. Zhang, D. Wang, D. Xu, Morphology investigation of transcrystallinity at polyamide 66/aramid fiber interface, J. Appl. Polym. Sci. 91 (2004) 2980–2983, https://doi.org/10.1002/app.13500.

[43] A. Feldman, M.F. Gonzalez, G. Marom, Transcrystallinity in surface modified aramid fiber reinforced nylon 66 composites, Macromol. Mater. Eng. 288 (2003) 861–866, https://doi.org/10.1002/mame.200300151, 2003.

[44] N. Klein, G. Marom, E. Wachtel, Microstructure of nylon 66 transcrystalline layers in carbon and aramid fibre reinforced composites, Polymer 37 (1996) 5493–5498, https://doi.org/10.1016/S0032-3861(96)00361-8.

[45] T. Elzein, M. Brogly, J. Schultz, Crystallinity measurements of polyamides adsorbed as thin films, Polymer 43 (2002) 4811–4822, https://doi.org/10.1016/S0032-3861(02)00239-2.

[46] C.W. Bunn, E.V. Garner, W.L. Bragg, The crystal structures of two polyamides ("nylons"), Proc. R. Soc. Lond. Ser. Math. Phys. Sci. 189 (1947) 39–68, https://doi.org/10.1098/rspa.1947.0028.

[47] C. Ramesh, New crystalline transitions in nylons 4,6, 6,10, and 6,12 using high temperature X-ray diffraction studies, Macromolecules 32 (1999) 3721–3726, https://doi.org/10.1021/ma981284z.

[48] E.G. Chatzi, J.L. Koenig, Morphology and structure of kevlar fibers: a review, Polym.-Plast. Technol. Eng. 26 (1987) 229–270, https://doi.org/10.1080/03602558708071938.

[49] S. Rojstaczer, D. Cohn, G. Marom, Thermal expansion of Kevlar fibres and composites, J. Mater. Sci. Lett. 4 (1985) 1233–1236, https://doi.org/10.1007/BF00723467.

[50] D. Ahmed, Z. Hongpeng, K. Haijuan, L. Jing, M. Yu, Y. Muhuo, Microstructural developments of poly (p-phenylene terephthalamide) fibers during heat treatment process: a review, Mater. Res. 17 (2014) 1180–1200, https://doi.org/10.1590/1516-1439.250313.

[51] R.A. Weiss, W. Huh, L. Nicolais, Novel reinforced polymers based on blends of polystyrene and a thermotropic liquid crystalline polymer, Polym. Eng. Sci. 27 (1987) 684–691, https://doi.org/10.1002/pen.760270913.

[52] F. Ansari, S. Galland, M. Johansson, C.J.G. Plummer, L.A. Berglund, Cellulose nanofiber network for moisture stable, strong and ductile biocomposites and increased epoxy curing rate, Compos. Part Appl. Sci. Manuf. 63 (2014) 35–44, https://doi.org/10.1016/j.compositesa.2014.03.017.

[53] A.J. Lovinger, Crystallographic factors affecting the structure of polymeric spherulites. II. X-ray diffraction analysis of directionally solidified polyamides and general conclusions, J. Appl. Phys. 49 (1978) 5014–5028, https://doi.org/10.1063/1.324448.

[54] L. Tang, C. Weder, Cellulose whisker/epoxy resin nanocomposites, ACS Appl. Mater. Interfaces 2 (2010) 1073–1080, https://doi.org/10.1021/am900830h.

[55] I.M. Ward, Structure and Properties of Oriented Polymers, Springer Science & Business Media, 2012.

[56] Y. Zare, An approach to study the roles of percolation threshold and interphase in tensile modulus of polymer/clay nanocomposites, J. Colloid Interface Sci. 486 (2017) 249–254, https://doi.org/10.1016/j.jcis.2016.09.080.

[57] X. Fu, S. Qutubuddin, Polymer–clay nanocomposites: exfoliation of organophilic montmorillonite nanolayers in polystyrene, Polymer 42 (2001) 807–813, https://doi.org/10.1016/S0032-3861(00)00385-2.

[58] C.Y. Yue, G.X. Sui, H.C. Looi, Effects of heat treatment on the mechanical properties of Kevlar-29 fibre, Compos. Sci. Technol. 60 (2000) 421–427, https://doi.org/10.1016/S0266-3538(99)00137-2.

[59] O. Monticelli, D. Oliva, S. Russo, C. Clausnitzer, P. Pötschke, B. Voit, On blends of polyamide 6 and a hyperbranched aramid, Macromol. Mater. Eng. 288 (2003) 318–325, https://doi.org/10.1002/mame.200390033.

[60] A. Mathur, A.N. Netravali, Mechanical property modification of aramid fibers by polymer infiltration, Textil. Res. J. 66 (1996) 201–208, https://doi.org/10.1177/004051759606600403.

[61] H. Kong, Q. Xu, M. Yu, Microstructural changes of aramid fiber due to reaction with toluene 2,4-diisocyanate under tension in $scCO_2$, Polymers 11 (2019) 1110, https://doi.org/10.3390/polym11071110.

[62] R. Groote, M. Baus, J.G.P. Goossens, Dynamic Cross-Linked Poly (Amides) Prepared via the Incorporation of Polyamines/Ammonium Salts in the Solid State, 2018. U.S. Patent 20180201732.

[63] Nylon 610, Glass reinforced product list. http://lookpolymers.com/category_Nylon-610-Glass-Reinforced.php. (Accessed 19 April 2023).

[64] Y. Peng, D.J. Gardner, Y. Han, Characterization of mechanical and morphological properties of cellulose reinforced polyamide 6 composites, Cellulose 22 (2015) 3199–3215, https://doi.org/10.1007/s10570-015-0723-y.

[65] A. Nicharat, J. Sapkota, C. Weder, E.J. Foster, Melt processing of polyamide 12 and cellulose nanocrystals nanocomposites, J. Appl. Polym. Sci. 132 (2015), 42752, https://doi.org/10.1002/app.4275.